# Conservation Voltage Reduction with Distributed Energy Resource Management System, Grid-Edge, and Legacy Devices

## Preprint

Harsha Padullaparti, Murali Baggu, Jing Wang, Ismael Mendoza, Soumya Tiwari, Jiyu Wang, and Santosh Veda

*National Renewable Energy Laboratory*

*Presented at the 2023 IEEE Power and Energy Society General Meeting*
*Orlando, Florida*
*July 16-20, 2023*

**NREL is a national laboratory of the U.S. Department of Energy**
**Office of Energy Efficiency & Renewable Energy**
**Operated by the Alliance for Sustainable Energy, LLC**

This report is available at no cost from the National Renewable Energy Laboratory (NREL) at www.nrel.gov/publications.

Contract No. DE-AC36-08GO28308

**Conference Paper**
NREL/CP-5D00-84633
July 2023

# Conservation Voltage Reduction with Distributed Energy Resource Management System, Grid-Edge, and Legacy Devices

## Preprint

Harsha Padullaparti, Murali Baggu, Jing Wang, Ismael Mendoza, Soumya Tiwari, Jiyu Wang, and Santosh Veda

*National Renewable Energy Laboratory*

**Suggested Citation**
Padullaparti, Harsha, Murali Baggu, Jing Wang, Ismael Mendoza, Soumya Tiwari, Jiyu Wang, and Santosh Veda. 2023. *Conservation Voltage Reduction with Distributed Energy Resource Management System, Grid-Edge, and Legacy Devices: Preprint*. Golden, CO: National Renewable Energy Laboratory. NREL/CP-5D00-84633.
https://www.nrel.gov/docs/fy23osti/84633.pdf



**NREL is a national laboratory of the U.S. Department of Energy**
**Office of Energy Efficiency & Renewable Energy**
**Operated by the Alliance for Sustainable Energy, LLC**

This report is available at no cost from the National Renewable Energy Laboratory (NREL) at www.nrel.gov/publications.

Contract No. DE-AC36-08GO28308

**Conference Paper**
NREL/CP-5D00-84633
July 2023

National Renewable Energy Laboratory
15013 Denver West Parkway
Golden, CO 80401
303-275-3000 • www.nrel.gov

## NOTICE

This work was authored by the National Renewable Energy Laboratory, operated by Alliance for Sustainable Energy, LLC, for the U.S. Department of Energy (DOE) under Contract No. DE-AC36-08GO28308. Funding provided by the U.S. Department of Energy Office of Energy Efficiency and Renewable Energy Solar Energy Technologies Office. The views expressed herein do not necessarily represent the views of the DOE or the U.S. Government. The U.S. Government retains and the publisher, by accepting the article for publication, acknowledges that the U.S. Government retains a nonexclusive, paid-up, irrevocable, worldwide license to publish or reproduce the published form of this work, or allow others to do so, for U.S. Government purposes.



*Cover Photos by Dennis Schroeder: (clockwise, left to right) NREL 51934, NREL 45897, NREL 42160, NREL 45891, NREL 48097, NREL 46526.*

# Conservation Voltage Reduction with Distributed Energy Resource Management System, Grid-Edge, and Legacy Devices

Harsha Padullaparti, Murali Baggu, Jing Wang, Ismael Mendoza, Soumya Tiwari, Jiyu Wang, Santosh Veda
National Renewable Energy Laboratory (NREL), Golden, Colorado, USA
HarshaVardhana.Padullaparti@nrel.gov; Murali.Baggu@nrel.gov

***Abstract*—Distribution utilities use conservation voltage reduction (CVR) to obtain energy savings and lower peak demand by reducing bus voltages. Traditionally, the CVR is accomplished by controlling the legacy assets such as load tap changers, voltage regulators, and capacitor banks. The deployment of the advanced distribution management system (ADMS) and distributed energy resource management system (DERMS) enables the integration of distributed energy resources into the distribution networks and provide the grid services including CVR. This paper studies the coordinated operation of an ADMS and a DERMS in achieving CVR and voltage regulation. A commercial ADMS uses legacy devices and Edge-of-Network Grid Optimization (ENGO) devices to obtain energy savings through CVR. A prototype DERMS dispatches the photovoltaic smart inverters based on real-time optimal power low to ensure voltage regulation across the feeder. The results show that the coordinated operation of ADMS and DERMS is effective in achieving CVR and voltage regulation. Specifically, energy savings of up to 4.7% are observed in the real utility distribution system used in this study.**

***Keywords—Advanced distribution management system, conservation voltage reduction, distributed energy resource management system, optimal power flow, voltage regulation.***

## I. Introduction

The global concerns over climate change, government policies and incentives in support of distributed energy resources (DERs), and the dramatic price reduction of DER technologies are accelerating the growth of DER penetration levels in distribution networks [1]. As a result, increased numbers of DERs—such as photovoltaic systems (PV), battery energy storage systems (BESS), electric vehicles (EV), fuel cells, and wind turbines—are expected to be integrated with the distribution grids. The increased DER penetration levels can lead to issues including over/under voltages, reverse power flows, overloading, and protection miscoordination. Nevertheless, when suitable controls are exercised, the DERs can provide various benefits such as improved network reliability, resiliency, voltage profile, reduced demand charges, and network losses.

State-of-the-art grid automation solutions such as advanced distribution management systems (ADMS) and distributed energy resource management systems (DERMS) [2], individually or in combination, can leverage the DERs to improve distribution grid operations. The ADMS offers the distribution operator advanced grid management functions such as Volt-VAR optimization (VVO), fault management, and outage management to improve situational awareness and optimize network operations [3]. The ADMS solutions typically control legacy devices such as load tap changers (LTC), voltage regulators (VRs), capacitor banks, and utility-scale DERs. Traditionally, the ADMS solutions do not have the visibility of or control over the behind-the-meter (BTM) DERs [2]. By contrast, the DERMS solutions aggregate the small-scale BTM DERs to provide grid services including demand response, voltage regulation, and situational awareness. The ADMS and DERMS solutions can complement each other to provide additional benefits [3].

Conservation voltage reduction (CVR) and voltage regulation are two of the key drivers for the distribution utilities for the deployment of ADMS and/or DERMS. CVR refers to lowering the load energy consumption by reducing the bus voltages. Many distribution utilities including Bonneville Power Administration, BC Hydro, and Southern California Edison studied the benefits of CVR in obtaining energy savings and reducing the peak demand [4]. However, these works did not consider the impact of DERs on CVR. The studies that considered the impact of DERs [5], [6] did not consider the coordination with the existing enterprise controls such as ADMS. As the distribution grid operations are transitioning towards the integration of ADMS and DERMS, realistic studies are needed that consider real distribution feeder models and coordinated control with ADMS and/or DERMS to help the utilities in de-risking the deployment of such technologies in the field. The works reported that studied the ADMS-DERMS coordination [7]–[9] focused on demonstrating the voltage regulation only.

To address the specified research gaps, this paper evaluates the performance of the coordinated operation of ADMS and DERMS in performing CVR while enforcing voltage regulation. Schneider Electric's ADMS is interfaced with a prototype DERMS [10]–[12] using industry-standard protocols for this evaluation. The real-time optimal power flow algorithm developed in [10], which uses network information and voltage and power measurement feedback for the voltage regulation controls is used for the prototype DERMS. The detailed distribution network model developed based on the data from Xcel Energy is used in this study. This network includes Sentient Energy's edge-of-network optimization (ENGO) devices [3] that act as the distributed controllable Volt-VAR resources to support CVR and voltage regulation.

This work was authored by the National Renewable Energy Laboratory, managed and operated by Alliance for Sustainable Energy, LLC for the U.S. Department of Energy (DOE) under Contract No. DE-AC36-08GO28308. Funding provided by the U.S. Department of Energy Office of Energy Efficiency and Renewable Energy Solar Energy Technologies Office. The views expressed in the article do not necessarily represent the views of the DOE or the U.S. Government. The U.S. Government retains and the publisher, by accepting the article for publication, acknowledges that the U.S. Government retains a nonexclusive, paid-up, irrevocable, worldwide license to publish or reproduce the published form of this work, or allow others to do so, for U.S. Government purposes.

The main contributions of this work are:

1. Evaluation and demonstration of the coordinated operation of ADMS and prototype DERMS to accomplish CVR and voltage regulation in the presence of high PV generation (nearly 200% relative to minimum load). Co-simulations of real-world distribution feeder models, a commercial ADMS, and a DERMS are performed to keep the study realistic.

2. Analyze and quantify the benefits of CVR based on simulation results, showing the advantages of using coordinated control of ADMS and DERMS for managing future grids with high renewables.

3. Provide the distribution utilities with insights into the expected benefits of ADMS and DERMS deployments, especially in the presence of high levels of distributed PV.

## II. Distribution Network Modeling

### A. Distribution System Details

A detailed distribution feeder model developed based on the data from the utility Xcel Energy is used for the demonstrations in this study. This is a 12.47-kV distribution network with a peak load of nearly 35 MW, located in Colorado within the service territory of the utility. The topology of the network is shown in Fig. 1. The legacy devices on this network for voltage regulation include a load tap changer at the substation and 13 switched capacitor banks installed as highlighted in Fig. 1. Each capacitor bank is rated for 1.2 Mvar. Further, there are 144 Edge-of-Network Grid Optimization (ENGO) devices [3] installed on this distribution network at the locations marked as grid-edge devices in Fig. 1. The ENGO devices are installed on the low-voltage side of the service transformers and act as low-voltage static compensators to regulate their terminal voltages. Based on the configurable voltage regulation setpoints, these devices provide dynamic reactive power compensation to improve the network voltage profile [3]. The loads are modeled as ZIP loads to account for the voltage dependency. The ZIP coefficients [0.24, 0.36, 0.4] are selected based on [13] and a pilot study conducted by another utility and are used for the load modeling. A realistic high PV penetration scenario is generated by distributing the PV systems randomly across the feeder with the PV sizes ranging from 1 kW to 10 kW. The PV profiles are created based on the solar irradiance information from the solar irradiance database recorded at NREL Flatirons Campus [14]. A subtree of the distribution network, encircled in red in Fig. 1, is modeled in OPAL-RT.

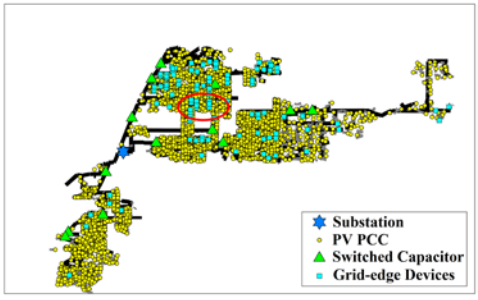


Fig. 1. Topology of the distribution feeder.

### B. Volt-VAR-Watt Curve Settings and Emulation

When the PV smart inverters are configured to function in autonomous local control mode (scenario S1 in Section IV), they are assumed to follow the Volt-VAR-Watt curve constituting the Volt-VAR and Volt-Watt curves shown in Fig. 2. The settings of IEEE 1547 Volt-VAR curve and California rule 21 Volt-Watt curve shown in Tables I and II are used for these curves. In the Volt-VAR-Watt mode, the PV smart inverter real and reactive power outputs are determined simultaneously by the Volt-VAR and Volt-Watt curves shown in Fig. 2. As the Volt-VAR-Watt smart inverter control function is not available in OpenDSS, we developed a Python function to implement this control.

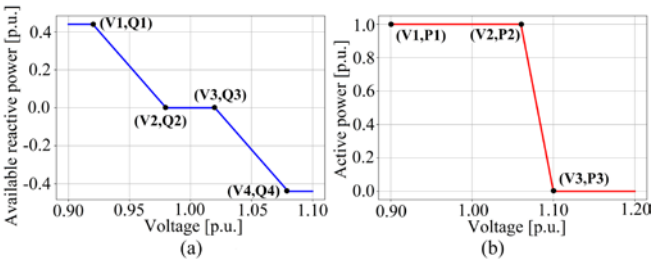


Fig. 2. (a) Volt-VAR curve, and (b) Volt-Watt curve.

TABLE I
VOLT-VAR CURVE SETTINGS

| Curve | V1 | Q1 | V2 | Q2 | V3 | Q3 | V4 | Q4 |
|---|---|---|---|---|---|---|---|---|
| Volt-VAR | 0.92 | 0.44 | 0.98 | 0 | 1.02 | 0 | 1.08 | -0.44 |

TABLE II
VOLT-WATT CURVE SETTINGS

| Curve | V1 | P1 | V2 | P2 | V3 | P3 |
|---|---|---|---|---|---|---|
| Volt-Watt | 0.9 | 1 | 1.05 | 1 | 1.1 | 0 |

### C. Prototype DERMS

A prototype DERMS based on the real-time optimal power flow algorithm (RT-OPF) [11], [15] is used in this work to control PV smart inverters. The details of the RT-OPF formulation are provided in this section.

Consider that $\mathcal{N} := \{1, \dots, N\}$ is the set of nodes in a distribution network, and $\mathcal{N}^{PV} \subseteq \mathcal{N}$ is the set of nodes where the smart PV inverters are connected. Let $\boldsymbol{X}^t := \{p_j^t, q_j^t, j \in \mathcal{N}^{PV}\}$ be vector of actual active ($p_j^t$) and reactive ($q_j^t$) power outputs from $j^{th}$ PV inverter at time $t$. Let $S_j$ be the $j^{th}$ PV inverter rating. Then, the RT-OPF problem can be defined as:

$$min\ f(\boldsymbol{X}^t) = \sum_{j \in \mathcal{N}^{PV}} w_p.(p_j^{t,max} - p_j^t)^2 + w_q.(q_j^t)^2 \quad (1a)$$

$$s.t. \quad 0 \le p_j^t \le p_j^{t,max}, \quad (1b)$$

$$(p_j^t)^2 + (q_j^t)^2 \le {S_j}^2, \quad (1c)$$

$$\underline{v}^t \le |v_n^t| \le \bar{v}^t, n \in \mathcal{N}. \quad (1d)$$

The first term in objective (1a) minimizes the active power curtailment and the second term minimizes the reactive power output from all the PV inverters. The weights $w_p$ and $w_q$ set the relative weights of these two terms ($w_p \gg w_q$). The active power production by $j^{th}$ PV inverter at time $t$ is limited by $p_j^{t,max}$ based on the irradiance level. The constraint (1c) ensures the inverter power output remains within the apparent power rating and (1d) drives the node voltages to remain within the ANSI limits.

Let $\boldsymbol{V}$ be the complex node voltages, $|\boldsymbol{V}|$ be the node voltage magnitudes, $\boldsymbol{p}_{inj}$ and $\boldsymbol{q}_{inj}$ be the active and reactive power injection vectors, respectively. Then, based on the linear power flow model proposed in [16], the linear approximation of $\boldsymbol{V}$ and $|\boldsymbol{V}|$ can be expressed as:

$$\boldsymbol{V} = \boldsymbol{A}\boldsymbol{p}_{inj} + \boldsymbol{B}\boldsymbol{q}_{inj} + \boldsymbol{k}, \quad (2a)$$

$$|\boldsymbol{V}| = \boldsymbol{C}\boldsymbol{p}_{inj} + \boldsymbol{D}\boldsymbol{q}_{inj} + \boldsymbol{l}, \quad (2b)$$

where $\boldsymbol{A}$, $\boldsymbol{B}$, $\boldsymbol{C}$, and $\boldsymbol{D}$ are the power coefficient matrices, and $\boldsymbol{k}$ and $\boldsymbol{l}$ are the constant vectors representing error terms. The RT-OPF problem (1) is solved by the primal-dual gradient algorithm with voltage measurement feedback. Let the Lagrangian function of problem (1) at time $t$ be $\mathcal{L}^t\left(\boldsymbol{X}^t, \overline{\boldsymbol{\mu}}^t, \underline{\boldsymbol{\mu}}^t\right)$, where $\overline{\boldsymbol{\mu}}^t$ and $\underline{\boldsymbol{\mu}}^t$ denote the Lagrangian multipliers for the upper and lower voltage limit constraints, respectively. Then the PV inverter power setpoints for the next control time window ($t+1$) can be solved as:

$$\boldsymbol{X}^{(\boldsymbol{t+1})} = Proj\left\{\boldsymbol{X}^{\boldsymbol{t}} - \alpha_x . \nabla_x \mathcal{L}\left(\boldsymbol{X}^t, \overline{\boldsymbol{\mu}}^t, \underline{\boldsymbol{\mu}}^t\right)\right\}. \quad (3)$$

where $\alpha_x$ is the constant step size, and $\nabla_x \mathcal{L}$ is the gradient. The Lagrangian multipliers are updated as:

$$\overline{\boldsymbol{\mu}}^t = Proj\left\{\overline{\boldsymbol{\mu}}^{(t-1)} + \alpha_{\overline{\mu}} . \nabla_{\overline{\mu}} \mathcal{L}\left(\boldsymbol{v}^{(t-1)} | \boldsymbol{X}^{(t-1)}\right)\right\}, \quad (4a)$$

$$\underline{\boldsymbol{\mu}}^t = Proj\left\{\underline{\boldsymbol{\mu}}^{(t-1)} + \alpha_{\underline{\mu}} . \nabla_{\underline{\mu}} \mathcal{L}\left(\boldsymbol{v}^{(t-1)} | \boldsymbol{X}^{(t-1)}\right)\right\}, \quad (4b)$$

where $\alpha_{\overline{\mu}}$ and $\alpha_{\underline{\mu}}$ are the constant step sizes, $\nabla_{\overline{\mu}}$ and $\nabla_{\underline{\mu}}$ are the gradients which can be computed based on the voltage measurement feedback vector $\boldsymbol{v}^{(t-1)}$ at previous time step. The gradient $\nabla_x \mathcal{L}$ is a function of $\boldsymbol{X}^{(t-1)}$, $\overline{\boldsymbol{\mu}}^{(t-1)}$, $\underline{\boldsymbol{\mu}}^{(t-1)}$, $\boldsymbol{A}$, $\boldsymbol{B}$, $\boldsymbol{C}$, and $\boldsymbol{D}$. The gradient descent algorithm is used to solve the optimization. The equations (3) and (4) are solved iteratively.

## III. Experimental Setup

The schematic of the experimental setup used for this study is shown in Fig. 3. It consists of Schneider Electric ADMS, the distribution network modeled in OpenDSS and OPAL-RT, the RTOPF algorithm implemented in Python, a real-time automation controller (RTAC), and the test bed coordinator software implemented in Python. In our setup, the ADMS runs the Volt-VAR Optimization (VVO) at every 5-minute intervals to compute the optimal voltage regulation set point for LTC and on/off statuses for all the medium-voltage capacitor banks. The ADMS VVO is a model-based multi-objective constrained optimization procedure, with user-definable optimization criteria and constraints. The ADMS VVO objectives include customer voltage improvement (voltage regulation) and CVR. In this work, the CVR is selected as the VVO objective. The medium voltage lower and upper constraints are selected as 116 V and 126 V, respectively on a 120 V base. The ADMS VVO tries to maintain the bus voltages on the primary distribution network within these voltage limits with a deadband of 0.6 V. The low voltage lower and upper constraints are 114 V and 126 V, respectively. These voltage limits are applicable to the bus voltages in the low-voltage secondary distribution network.

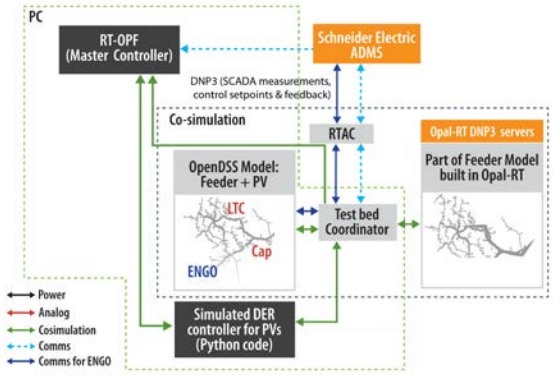


Fig. 3. Schematic of the experimental setup.

The distribution network power flow is solved in OpenDSS and OPAL-RT together at each time step as described in [3]. The time step resolution is selected as 5-second. The measurements from the power flow are communicated to the ADMS as simulated SCADA at each 5-second interval via RTAC. These measurements include real power, reactive power, line currents at the feeder head, reactive power injection, and the terminal voltages of the ENGO devices. The simulated SCADA measurements are used by the ADMS to estimate the network status through state estimation. The RTAC acts as a substation gateway to establish the communication between ADMS and OpenDSS. It performs the UDP to DNP3 protocol translation to pass the measurement data from OpenDSS to ADMS because OpenDSS can only support UDP. Further, the ADMS sends the LTC and capacitor bank set points to OpenDSS at 5-minute intervals through RTAC. The RTAC performs DNP3 to UDP protocol translation for this.

A co-simulation manager developed in Python referred to as the test bed coordinator, is used to perform the co-simulations. The test bed coordinator is responsible for implementing the simulated device set points in OpenDSS such as the LTC and ENGO device voltage regulation set points and capacitor bank on/off statuses based on the signals received from ADMS, setting the simulated PV smart inverter powers based on the set points computed by RTOPF.

## IV. Results and Discussion

The coordinated ADMS-DERMS operation for CVR is demonstrated using three scenarios summarized in Table III. In the baseline scenario, the legacy devices, i.e., the LTC and the capacitor banks are in the local control mode. The ENGO units are disabled and all the PV systems are set to operate in the unity power factor mode. In the S1 scenario, the set points for the legacy devices and the ENGO devices are issued by the ADMS. The PV smart inverters are configured to work in Volt-VAR-Watt control mode with the curves shown in Fig. 2. In S2, the PV smart inverters are dispatched by the RTOPF. The legacy devices and the ENGO units receive the set points from the ADMS. Based on the historical SCADA data, a day having the minimum load with excessive PV generation is selected for the simulations in this study. In this section, the results in each scenario for the minimum load day are discussed in detail.

TABLE III
Simulation Scenarios

| Scenario | Legacy Devices | ENGO units | PV Smart Inverters |
|---|---|---|---|
| **Baseline** | Local control | - | Unity power factor |
| **S1** | ADMS | ADMS | Local Volt-VAR-Watt control mode |
| **S2** | ADMS | ADMS | RTOPF |

The performance of the coordinated operation of ADMS and DERMS in performing the CVR and the voltage regulation controls is evaluated using the following metrics:

1. *Energy delivered by substation (MWh):* This is the total energy delivered by the substation.
2. *Energy delivered by PV (MWh):* This is the total energy export from all the PV systems to the feeder.
3. *Energy savings (in MWh and %):* This is the energy savings observed in S1 or S2 compared to the baseline, expressed in MWh and as a percentage of energy delivered by the substation in the baseline.
4. Voltage exceedances, $T_{ex}$ *(in node-hours):* The voltage magnitude of a bus being outside of the ANSI voltage

range of 0.95 p.u. – 1.05 p.u. is referred to as voltage exceedance. A bus can have multiple phases and each phase is considered a node. Thus, a three-phase bus has three nodes, and a single-phase bus has one node. The number of nodes exceeding the ANSI limits is multiplied by duration of exceedances and expressed as node-hours.

### A. *Baseline Scenario Results*

The results from the baseline scenario are shown in Fig. 4. The bus voltages shown in Fig. 4(a) indicate that there are many buses experiencing overvoltage issues due to high PV generation, specifically during the time period from time 8:00 to 14:00. The fast voltage variations due to the PV generation variabilities are also observed during this period. The peak PV generation is approximately 30 MW from the total PV generation plot in Fig. 4(b). More than 10 MW of reverse power flow is observed at the substation in Fig. 4(c) due to the high PV generation. The capacitor statuses are shown in Fig. 4(d) in which the 'on' status is marked by the blue bar. For example, Cap 5 is on during the initial few hours, and Cap 4 is on throughout the simulated day. The LTC tap position remained fixed at position 0 throughout the day (not shown).

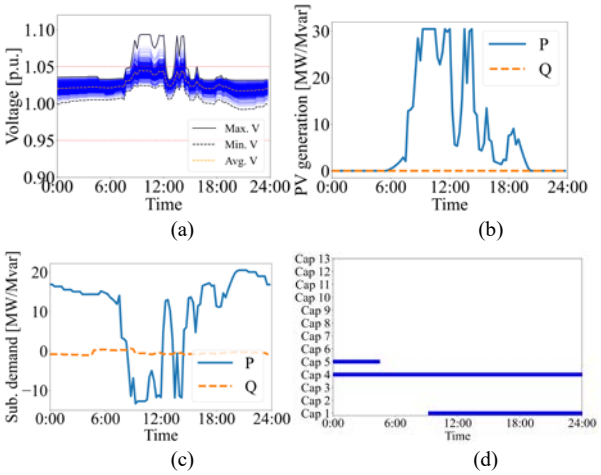


Fig. 4. Baseline results: (a) bus voltages, (b) total PV generation, (c) substation demand, and (d) capacitor bank statuses.

### B. *S1 Scenario Results*

In the S1 scenario, the LTC and the ENGO units follow the same voltage regulation set points received from the ADMS. The voltage regulation set point changes on the 120 V base and the corresponding LTC tap position changes are shown in Fig. 5(a). The ADMS lowered the set point to nearly 120 V at around time 3:00 for reducing the system voltages to exercise CVR. As a result, the LTC tap position is lowered to - 6. The bus voltages shown in Fig. 5(b) indicate that the voltages are reasonably restricted to the lower ANSI band of 0.95 p.u. – 1.0 p.u. during the period when high PV generation is not present. Additionally, the overvoltages above 1.05 p.u. are resolved primarily due to the ADMS lowering the LTC tap position. The total reactive power injection from all 144 ENGOs is shown in Fig. 5(c). The ENGOs injected nearly 1,350 kvar reactive power during the initial 3 hours of the simulation. The reactive power output from the ENGO devices dynamically varied to compensate for the voltage dynamics due to the PV power variabilities. The capacitor bank statuses, shown in Fig. 5(d), indicate that many capacitor banks compared to the baseline are turned on by the ADMS.

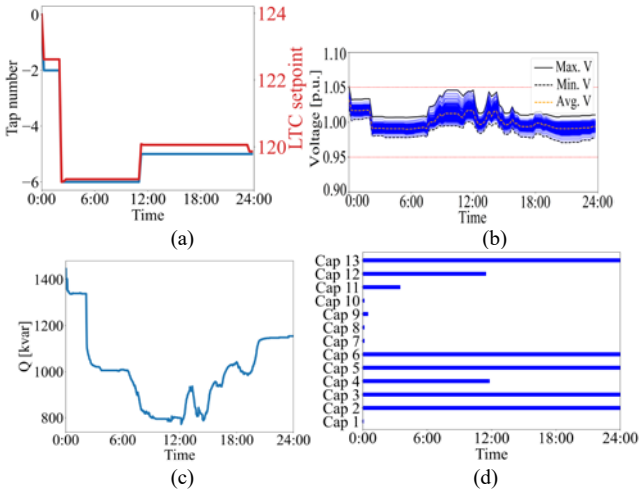


Fig. 5. S1 results: (a) LTC set point and tap changes, (b) bus voltages, (c) total reactive power output ENGO units, and (d) capacitor bank statuses.

### C. *S2 Scenario Results*

The LTC set point changes from the ADMS in the S2 scenario, shown in Fig. 6(a), are similar to those in the S1 scenario. The ADMS lowered the LTC set point to nearly 119 V at the beginning of the simulation and the LTC tap reduced to -6. The tap stayed at this position for the rest of the simulation period, except for a brief period at around 18:00. As a result, the bus voltages shown in Fig. 6(b) are mostly confined to the lower ANSI band during the hours when significant PV generation is not present. The overvoltage issues are also resolved in this scenario.

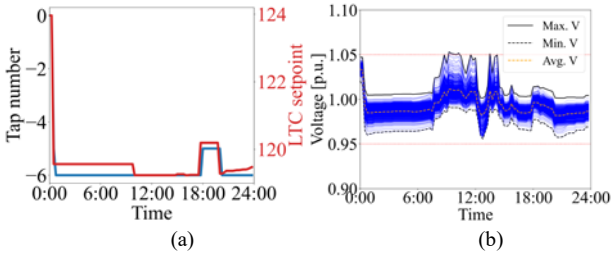


Fig. 6. S2 results: (a) LTC set point and tap changes, and (b) bus voltages.

The capacitor bank statuses in S2 are shown in Fig. 7(a). It is evident that the ADMS kept many capacitor banks on in S2 also compared to the baseline. The total PV generation in the three scenarios is shown in Fig. 7(b). Note that the negative reactive power represents the reactive power absorption. It is observed that the active power curtailment in both scenarios S1 and S2 is negligible. The reactive power absorption of up to 3.5 Mvar by the PV smart inverters is observed in S2.

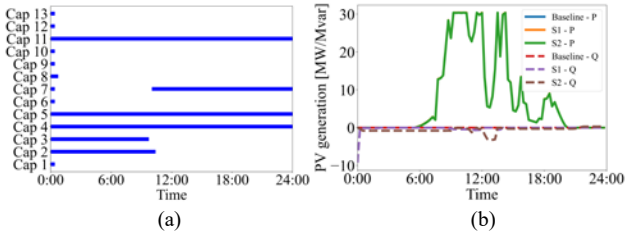


Fig. 7. (a) capacitor bank statuses in S2, and (b) comparison of total PV generation in different scenarios.

### D. *Metrics*

The metrics computed for the minimum load day are shown in Fig. 8. In Fig. 8(a), the energy delivered by the substation is observed to be the highest at 231.99 MWh in the baseline scenario despite having full active power export from

the PV systems. This is due to the lack of CVR control by the ADMS in the baseline. The total energy export from the PV is 188.2 MWh in this scenario. In S1, the total energy delivered by the substation is 223.34 MWh which is less than that in the baseline. This reduction can be attributed to the lower power consumption by the loads due to lower bus voltages compared to the baseline, i.e., CVR energy savings. The energy export from the PV in S1 is the same as that in the baseline. In S2, the total energy export from the PV is observed to be the lowest at 187.74 MWh due to some PV curtailment which is 0.25% energy curtailment compared to the baseline. However, the total energy delivery from the substation is the lowest at 221.06 MWh in S2 since the bus voltages are lower than the other scenarios in S2 longer. The energy savings and the voltage exceedances observed on the minimum load day are shown in Fig. 8(b). The energy savings in S1 are 3.73% and those in S2 are 4.71%. Additionally, the voltage exceedances in the baseline are very high at 3178 node-hours compared to the other scenarios. The voltage exceedances in S1 and S2 are 18.5 and 15.25 node-hours, respectively. In the case of S1, they occurred during the initial few minutes of the simulation.

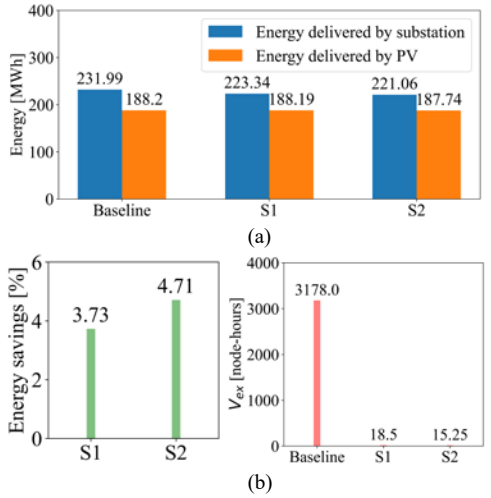


Fig. 8. Metrics for minimum load day.

## V. Conclusions

In this paper, we evaluated the coordinated operation of an ADMS and a prototype DERMS in achieving CVR while ensuring voltage regulation in a distribution network with high PV penetration. Different from most of the existing studies, this study uses a realistic experimental setup with a commercial ADMS, actual distribution network models from a utility partner, industry-standard communication interfaces, and co-simulations to replicate the utility control room environment as closely as possible. Our findings show that the ADMS lowers system voltages to achieve CVR by lowering the LTC taps which reduce the feeder head voltage. To prevent the resulting voltage drop across the network below the lower ANSI limit, the ADMS turns on the capacitor banks and also relies on the dynamic reactive power support from ENGO devices. The DERMS complements the ADMS in ensuring the voltage regulation through active and reactive power control of the PV smart inverters which have faster response time compared to LTC and capacitor banks in resolving the voltage issues. Energy savings of up to 4.7% with a significant improvement in the voltage profile and minimal PV energy export curtailment (0.25%) are observed in the studied system with these controls. As the utility industry is marching toward the deployment of ADMS and DERMS controls, the results of our study will provide them with insights into the expected benefits of such deployments. Our setup is flexible to study the performance of different ADMS, DERMS, and DER mixes. We will study the impact of other types of DERs as part of future work.

## Acknowledgment

The authors acknowledge the significant contributions of Fei Ding, Emiliano Dall'Anese, and Andrey Bernstein in algorithm development. The authors also thank Schneider Electric for supporting the ADMS configurations, Sentient Energy for supporting the GEMS and ENGO hardware and OpenDSS model setup, and Xcel Energy for providing operational insights and utility data.

## References

[1] B. Kroposki *et al.*, "Autonomous Energy Grids: Controlling the Future Grid With Large Amounts of Distributed Energy Resources," *IEEE Power and Energy Mag.*, vol. 18, no. 6, pp. 37–46, Nov. 2020.

[2] L. Strezoski, H. Padullaparti, F. Ding, and M. Baggu, "Integration of Utility Distributed Energy Resource Management System and Aggregators for Evolving Distribution System Operators," *Journal of Modern Power Systems and Clean Energy*, vol. 10, no. 2, 2022.

[3] H. Padullaparti, J. Wang, S. Veda, M. Baggu, and A. Golnas, "Evaluation of Data-Enhanced Hierarchical Control for Distribution Feeders With High PV Penetration," *IEEE Access*, vol. 10, 2022.

[4] Z. Wang and J. Wang, "Review on Implementation and Assessment of Conservation Voltage Reduction," *IEEE Transactions on Power Systems*, vol. 29, no. 3, pp. 1306–1315, May 2014.

[5] S. Singh, S. Veda, S. P. Singh, R. Jain, and M. Baggu, "Event-Driven Predictive Approach for Real-Time Volt/VAR Control With CVR in Solar PV Rich Active Distribution Network," *IEEE Transactions on Power Systems*, vol. 36, no. 5, pp. 3849–3864, Sep. 2021.

[6] F. Ding and M. Baggu, "Coordinated Use of Smart Inverters with Legacy Voltage Regulating Devices in Distribution Systems with High Distributed PV Penetration — Increase CVR Energy Savings," *IEEE Transactions on Smart Grid*, pp. 1–1, 2018.

[7] H. Padullaparti *et al.*, "Peak Load Management in Distribution Systems Using Legacy Utility Equipment and Distributed Energy Resources," in *2021 IEEE Green Technologies Conference (GreenTech)*, Denver, CO, USA, Apr. 2021, pp. 435–441.

[8] J. Wang, H. Padullaparti, S. Veda, I. Mendoza, S. Tiwari, and M. Baggu, "Performance Evaluation of Data-Enhanced Hierarchical Control for Grid Operations," in *IEEE Power & Energy Society General Meeting*, Montreal, QC, Canada, Aug. 2020, pp. 1–5.

[9] J. Wang, H. Padullaparti, F. Ding, M. Baggu, and M. Symko-Davies, "Voltage Regulation Performance Evaluation of Distributed Energy Resource Management via Advanced Hardware-in-the-Loop Simulation," *Energies*, vol. 14, no. 20, p. 6734, Oct. 2021.

[10] E. Dall'Anese, S. S. Guggilam, A. Simonetto, Y. C. Chen, and S. V. Dhople, "Optimal Regulation of Virtual Power Plants," *IEEE Transactions on Power Systems*, vol. 33, no. 2, Art. no. 2, 2018.

[11] F. Ding, H. Padullaparti, M. Baggu, and S. Veda, "Data-Enhanced Hierarchical Control to Improve Distribution Voltage with Extremely High PV Penetration," in *IEEE PES General Meeting*, 2019.

[12] F. Ding, "Distributed energy resource management solution using real-time optimization." NREL Software Record, SWR-20-46, 2019.

[13] M. S. Hossan and B. H. Chowdhury, "Exponential factor dependent ZIP coefficients extraction and impacts of CVR in a utility feeder," in *North American Power Symposium (NAPS)*, Oct. 2015, pp. 1–6.

[14] D. Jager and A. Andreas, "NREL national wind technology center (NWTC): M2 Tower; Boulder, Colorado (Data)," National Renewable Energy Lab. (NREL), No. NREL/DA-5500-56489.

[15] E. Dall'Anese and A. Simonetto, "Optimal Power Flow Pursuit," *IEEE Transactions on Smart Grid*, vol. 9, no. 2, p. 11, 2018.

[16] A. Bernstein and E. Dall'Anese, "Linear power-flow models in multiphase distribution networks," in *IEEE PES Innovative Smart Grid Tech. Conf. Europe*, Italy, 2017, pp. 1–6.